Full band calculations of the intrinsic lower limit of contact resistivity

J. Maassen,[1,a)] C. Jeong,[1] A. Baraskar,[2] M. Rodwell,[3] and M. Lundstrom[1]
[1]*Network for Computational Nanotechnology, School of Electrical and Computer Engineering, Purdue University, West Lafayette, Indiana 47907, USA*
[2]*GlobalFoundries, Yorktown Heights, New York 10598, USA*
[3]*Department of Electrical and Computer Engineering, University of California, Santa Barbara, California 93106, USA*

(Received 21 November 2012; accepted 8 March 2013; published online 21 March 2013)

The intrinsic lower limit of contact resistivity (ρ_c^{LL}) for InAs, $In_{0.53}Ga_{0.47}As$, GaSb, and Si is calculated using a full band ballistic quantum transport approach. Surprisingly, our results show that ρ_c^{LL} is almost independent of the semiconductor. An analytical model, derived for 1D, 2D, and 3D, correctly reproduces the numerical results and explains why ρ_c^{LL} is very similar in all cases. Our analysis sets a minimal carrier density required to meet the International Technology Roadmap for Semiconductors call for $\rho_c = 10^{-9}\,\Omega\text{-cm}^2$ by 2023. Comparison with experiments shows there is room for improvement, which will come from optimizing interfacial properties. © *2013 American Institute of Physics*. [http://dx.doi.org/10.1063/1.4798238]

Achieving ultra-low contact resistivities for metal/semiconductor junctions represents a significant obstacle for the scaling of nano-scale devices and the development of THz bandwidth high-speed transistors.[1] Much experimental effort has been devoted to producing high quality material interfaces, utilizing *in-situ* techniques for sample fabrication, with the goal of reducing the specific contact resistivity (ρ_c).[2] The International Technology Roadmap for Semiconductors (ITRS) has called for a contact resistivity of $10^{-9}\,\Omega\text{-cm}^2$ for 2023.[3] This leads us to ask the following question: What is the ultimate lower limit of Ohmic contact resistivity?

A recent theoretical study based on the parabolic approximation and realistic band profiles demonstrated contact resistivity values in excellent agreement with experiment.[4] This study also computed the case of perfect reflection-less contacts, and found that this resistance was within an order of magnitude of the lowest measured contact resistivity to n-InGaAs. To achieve lower ρ_c values, high doping concentrations are required, which can push the Fermi level far from the band edge where the electronic dispersion can be highly non-parabolic. In this work, we address this important issue by calculating the theoretical lower limit of contact resistivity (ρ_c^{LL}) for several semiconductors by combining accurate full band electronic structure calculations with the Landauer quantum transport formalism. By naturally taking into account the role of valley degeneracy, band anisotropy, higher energy bands, and the highly non-parabolic shape of the bands, our results allow us to quantitatively assess how much improvement in ρ_c is possible given the present experimental values and verify the validity of parabolic-based ρ_c models. An analytical model, applicable to 1D, 2D, and 3D structures, is found to adequately reproduce the full band numerical results and is utilized to provide an answer to what material properties are desired to achieve the lowest possible ρ_c^{LL}.

In this work, the intrinsic lower limit of metal/semiconductor contact resistivity is calculated assuming that (i) transport across the junction is ballistic, i.e., no scattering and no Schottky barrier for carriers to tunnel through, and that (ii) the metal is ideal meaning it contains more than enough conducting channels to supply the semiconductor. To compute ρ_c^{LL}, we use the Landauer approach, which is naturally suited to treat ballistic transport. The contact resistivity (or inverse of the conductance per unit area), defined in the limit of zero applied bias, can be expressed as[5]

$$\frac{1}{\rho_c^{LL}} = \frac{4q^2}{h}\int_{-\infty}^{+\infty} M(\epsilon)\left[-\frac{\partial f}{\partial \epsilon}\right]d\epsilon, \quad [\Omega^{-1}\text{–}m^{-2}], \qquad (1)$$

where q is the electron charge, h is Planck's constant, $M(\epsilon)$ is the semiconductor distribution of modes (DOMs) or number of conducting channels at energy ϵ, and f is the Fermi-Dirac distribution. The function $[-\partial f/\partial\epsilon]$ is centered at the Fermi level E_F and is strongly suppressed a few k_BT away from E_F, where k_B is Boltzmann's constant and T is the temperature. Thus, $(\rho_c^{LL})^{-1}$ can be simply interpreted as the number of "active" conducting channels times the quantum of conductance $2q^2/h$; an extra factor of two appears because half of the resistance is associated with each of the two contacts.

In this study, we consider four of the most important semiconductors for nano-scale and high-frequency electronic devices: InAs, $In_{0.53}Ga_{0.47}As$, GaSb, and Si. The first three are low-effective mass (m^*) III-V semiconductors with a single isotropic conduction band (CB) located at Γ, while Si has a six-fold degenerate large m^* anisotropic CB. By studying these much different semiconductors, our goal is to understand and identify characteristics that can lead to a reduction in contact resistivity. Fig. 1 presents the calculated band structures of InAs, $In_{0.53}Ga_{0.47}As$, GaSb, and Si using tight-binding and first principles frameworks (details found in figure caption). Most calculations of contact resistivity assume a parabolic-type form for the electronic bands, however at high doping concentrations, E_F may reside far from the band edge where features can be highly non-parabolic

a)Electronic address: jmaassen@purdue.edu

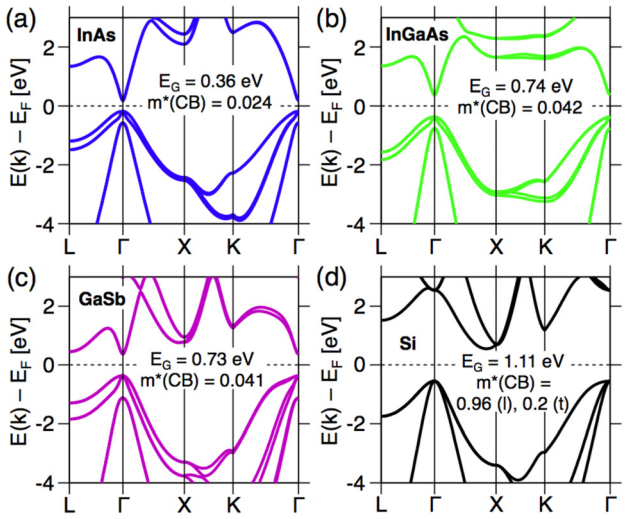

FIG. 1. Electronic band structure of InAs (a), $In_{0.53}Ga_{0.47}As$ (b), GaSb (c), and Si (d) along the high-symmetry points. (a)–(c) were calculated using a $sp^3d^5s^*$ tight-binding model as implemented in NEMO5.[8] (d) was obtained from VASP,[9] a density functional theory software package, using the generalized gradient approximation,[10] the experimental lattice constant of Si (5.43 Å) and applying the scissor technique to obtain the experimental band gap.

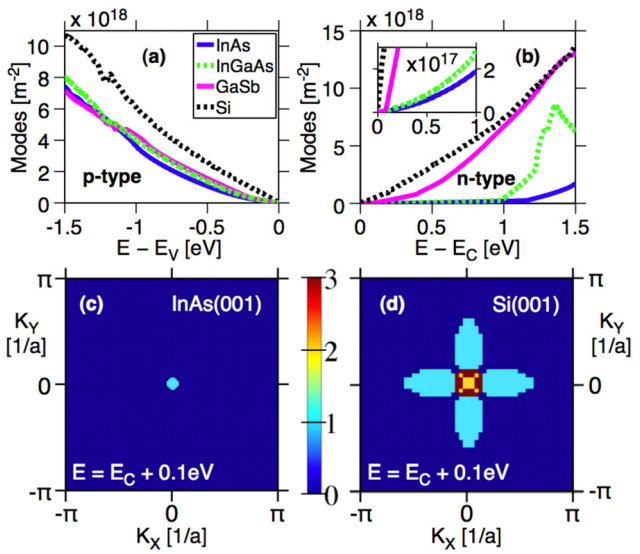

FIG. 2. DOM for the valence (a) and conduction (b) states of InAs $In_{0.53}Ga_{0.47}As$, GaSb, and Si. Energy is defined relative to the band edge. The number of conducting channels (modes) was calculated using Eq. (2). The inset of (b) shows the features of InAs and $In_{0.53}Ga_{0.47}As$ near the conduction edge and how GaSb increases rapidly at 0.1 eV due to a higher energy band with low m^*. (c) and (d): k-resolved DOM for the conduction band (0.1 eV) of InAs and Si. The shape of the plot indicates the projection of the iso-energy surface of the bands along the z-direction.

(as shown in Fig. 1) and higher energy bands may contribute to transport.

The full electronic dispersion serves as the input for calculating the DOM, which can be efficiently computed using the so-called "band-counting" method.[6] The number of conducting channels per unit area, at a given energy ϵ, is expressed as

$$M(\epsilon) = \frac{1}{(2\pi)^2}\int_{\mathrm{BZ}}\sum_{n^+}\Theta(\epsilon-\epsilon_{\mathbf{k}_\perp})\,\mathrm{d}\mathbf{k}_\perp, \quad [\mathrm{m}^{-2}], \qquad (2)$$

where $\Theta(\epsilon-\epsilon_{\mathbf{k}_\perp})$ is the Heaviside step function, $\mathbf{k}_\perp$ is the reciprocal vector in the plane perpendicular to transport, and n^+ is the number of forward moving states with energy ϵ and wavenumber $\mathbf{k}_\perp$. The integrand of Eq. (2) is an integer corresponding to the number of conducting channels, at a fixed ϵ and $\mathbf{k}_\perp$. For a non-parabolic Kane dispersion model,[7] where $\epsilon_{\mathbf{k}}(1+\alpha\epsilon_{\mathbf{k}}) = \hbar^2\mathbf{k}^2/2m^*$, the distribution of modes (for a 3D material) can be written analytically as $M(\epsilon) = m^*_{DOM}\epsilon(1+\alpha\epsilon)/2\pi\hbar^2$,[6] where α is the non-parabolicity parameter, $m^*_{DOM} = \sum_{g_v}\sqrt{m_x m_y}$ (transport along z-direction) is the DOM effective mass, g_v is the valley degeneracy, and ϵ is defined relative to the band edge. Thus, the number of conducting channels scales linearly with energy for parabolic bands ($\alpha = 0$) and quadratically with energy for non-parabolic bands ($\alpha \neq 0$).

Fig. 2 presents the distribution of modes, $M(\epsilon)$, for the valence and conduction states of InAs, $In_{0.53}Ga_{0.47}As$, GaSb, and Si. The p-type $M(\epsilon)$ is roughly the same for all semiconductors, with Si showing slightly larger values due to its comparatively smaller split-off energy and larger m^*. Significant differences in $M(\epsilon)$ appear for the conduction states. Si and GaSb have a much larger number of modes compared to InAs and $In_{0.53}Ga_{0.47}As$. For energies less than 1 eV, InAs and $In_{0.53}Ga_{0.47}As$ have a single low m^* band contributing to $M(\epsilon)$. According to the analytic expression shown above, $M(\epsilon)$ will scale linearly with m^*_{DOM}, which is simply m^* for an isotropic band.[14] For InAs and $In_{0.53}Ga_{0.47}As$, m^* is 0.024 m_0 and 0.042 m_0, respectively, where m_0 is the electron mass. While for Si, the longitudinal and transverse effective masses extracted from Fig. 1(d) are $m_l = 0.96$ m_0 and $m_t = 0.2$ m_0, leading to a m^*_{DOM} value of 2.15 m_0, considering a valley degeneracy of six. The difference in m^*_{DOM}, for InAs and $In_{0.53}Ga_{0.47}As$ versus Si, is the source of the roughly factor of 10^2 difference in DOM.

To better illustrate why small effective mass bands lead to a small DOM, in Figs. 2(c) and 2(d), we plot the $\mathbf{k}_\perp$-resolved DOM, i.e., the integrand in Eq. (2), for the conduction bands of InAs and Si. Such plots provide information on the projected iso-energy surface of the bands: a single small sphere for InAs and six large ellipsoids for Si. For a given energy, the InAs CB takes up only a small region in k-space, compared to the six bands of Si, which once projected along z and integrated leads to a small DOM. GaSb has a small effective mass CB with a m^* of 0.041 m_0, however a second large m^* band appears at 0.1 eV, which dramatically increases the DOM, as shown in the inset of Fig. 2(b). InAs and $In_{0.53}Ga_{0.47}As$ also have higher energy bands located at 1.17 eV and 0.98 eV above the band edge (according to Fig. 1), respectively, which result in sharp increases in $M(\epsilon)$.

In Figs. 3(a) and 3(b), contact resistivity ρ_c^{LL} versus carrier concentration (n) is presented for p-type and n-type InAs, $In_{0.53}Ga_{0.47}As$, GaSb, and Si. As the carrier concentration increases, the contact resistivity decreases. The roughly linear trend on the log-log plot indicates that ρ_c^{LL} is related to n via a power-law, $\rho_c^{LL} \propto n^x$, with $x \approx -2/3$ extracted from the slope. The main feature in Figs. 3(a) and 3(b) is that, for a fixed carrier concentration, ρ_c^{LL} is similar for all semiconductors (i.e., within a factor of 2–3). This is an unexpected result considering the very different DOM of each material, particularly for the conduction states. Plotting ρ_c^{LL} versus E_F,

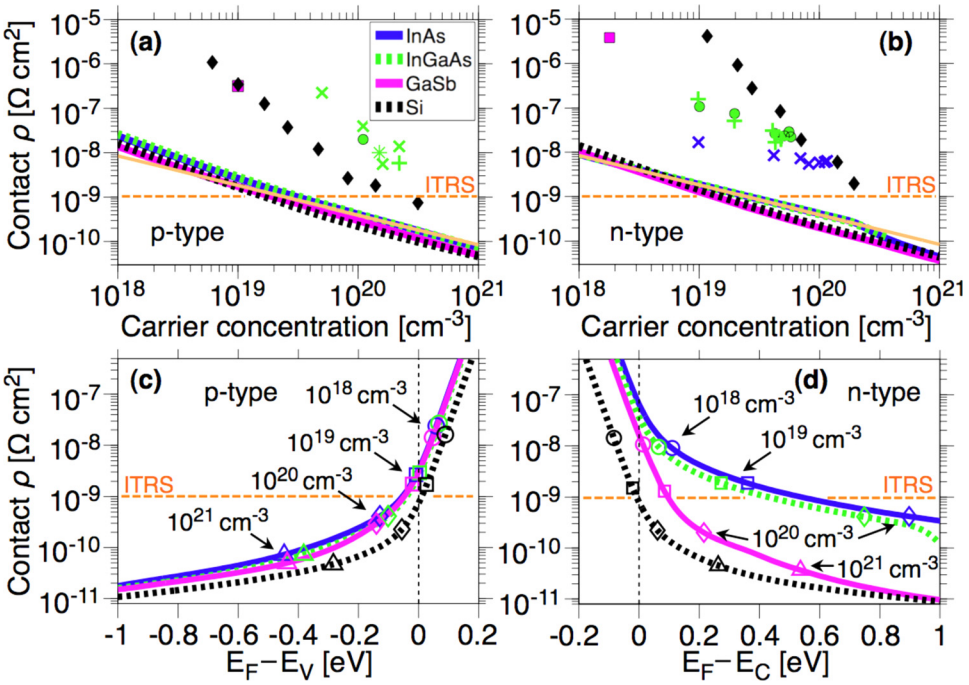

FIG. 3. Contact resistivity (ρ_c^{LL}) versus carrier concentration for p-type and n-type InAs, $In_{0.53}Ga_{0.47}As$, GaSb, and Si at 300 K. Markers are experimental data points taken from (InAs),[2] (InGaAs),[11] (GaSb),[12] and (Si).[13] Thin yellow solid line is the analytical expression with $m^*_{DOS}/m^*_{DOM} = 1$. (c)–(d): Contact resistivity versus E_F for p-type and n-type InAs, $In_{0.53}Ga_{0.47}As$, GaSb, and Si. E_F is defined relative to the valence and conduction band edges. Markers indicate the E_F values for carrier concentrations of 10^{18} (circle), 10^{19} (square), 10^{20} (diamond), and 10^{21} cm^{-3} (triangle). Dashed horizontal line corresponds to $\rho_c = 10^{-9}$ Ω-cm^2 called by the ITRS for 2023.

as shown in Figs. 3(c) and 3(d), confirms that semiconductors with a larger number of channels yield smaller ρ_c^{LL} values (for fixed E_F). The markers in Figs. 3(c) and 3(d), corresponding to carrier concentrations of 10^{18}, 10^{19}, 10^{20}, and 10^{21} cm^{-3}, indicate that it is the relationship between n and E_F, which leads to similar ρ_c^{LL} values for fixed n. In order to better understand the correspondence between ρ_c^{LL} and n, and why all the studied semiconductors have nearly the same ρ_c^{LL}, we will utilize an approximate analytical formula.

Lowering the contact resistivity requires high doping levels, which means the semiconductors are degenerate. In this case, one can safely evaluate ρ_c^{LL} (Eq. (1)) and the carrier concentration $n = \int_{-\infty}^{+\infty} D(\epsilon) f(\epsilon - E_F)\, d\epsilon$ in the $T = 0$ K limit.[14] Assuming a non-parabolic Kane model for the electronic dispersion in 3D, 2D, and 1D respectively, we find

$$\rho_c^{LL} = \frac{h}{4q^2}\frac{m^{3D}_{DOS}}{m^{3D}_{DOM}}\frac{4}{(3\sqrt{\pi}n^{3D})^{2/3}}, \quad [\Omega\text{–m}^2], \tag{3}$$

$$\rho_c^{LL} = \frac{h}{4q^2}\sqrt{\frac{\pi}{2}}\sqrt{\frac{m^{2D}_{DOS}}{m^{2D}_{DOM}}}\frac{1}{\sqrt{n^{2D}}}, \quad [\Omega - \text{m}], \tag{4}$$

$$\rho_c^{LL} = \frac{h}{4q^2}\frac{1}{g_v}, \quad [\Omega], \tag{5}$$

where $m^{3D}_{DOS} = [\sum_{g_v}\sqrt{m_x m_y m_z}]^{2/3}$, $m^{3D}_{DOM} = \sum_{g_v}\sqrt{m_x m_y}$, $m^{2D}_{DOS} = \sum_{g_v}\sqrt{m_y m_z}$ and $m^{2D}_{DOM} = [\sum_{g_v}\sqrt{m_y}]^2$ (assuming transport along z and confinement along x for the 2D case). The 3D and 2D carrier densities have units of m^{-3} and m^{-2}, respectively. Unless otherwise mentioned, we consider the case of 3D. Equation (3) predicts that ρ_c^{LL} should depend on n to the power −2/3 in the degenerate limit, as is observed with the numerical results. Note that the non-parabolicity parameter α does not appear in Eqs. (3)–(5), and that the ratio m^*_{DOS}/m^*_{DOM} is one for isotropic bands. Equation (3) is plotted in Figs. 3(a) and 3(b) as a thin yellow solid line, using $m^*_{DOS}/m^*_{DOM} = 1$, and is found to provide an excellent fit to the numerical results considering this simple equation depends only on fundamental constants. Thus, this model explains why the curves in Figs. 3(a) and 3(b) nearly overlap: any decrease in ρ_c^{LL} due to an increase in $M(\epsilon)$ is offset by a small E_F value relative to the band edge. Hence, a good conductor (large m^*_{DOM} and m^*_{DOS}) has a small E_F and a poor conductor (small m^*_{DOM} and m^*_{DOS}) has a large E_F, such that both yield a very similar ρ_c^{LL}. For Si, we have $m^*_{DOS}/m^*_{DOM} = 0.52$, which reduces ρ_c^{LL} compared to isotropic bands. As expected, comparing Si to InAs and $In_{0.53}Ga_{0.47}As$, we observe roughly a factor of two difference in ρ_c^{LL}. Finally, we highlight that the analytical expressions in Eqs. (3)–(5) predict that ρ_c^{LL} will have a gradually weaker dependence on carrier density, m^*_{DOM} and m^*_{DOS} as dimensionality is reduced.

We may ask how does valley degeneracy, band anisotropy, and higher energy bands affect the lower limit of ρ_c and why do such features, present in the full band calculations, do not induce significant differences in ρ_c^{LL} from one material to another. Assuming there are g_v degenerate ellipsoidal bands, Eq. (3) can be rewritten as

$$\rho_c^{LL} = \frac{h}{4q^2}\frac{1}{g_v^{1/3}}\left(\frac{m_z}{\sqrt{m_x m_y}}\right)^{1/3}\frac{4}{(3\sqrt{\pi}n)^{2/3}}, \quad [\Omega\text{–m}^2]. \tag{6}$$

We note that the same result, within a factor of two, was reported elsewhere.[4] Equation (6) indicates that although the lower limit of ρ_c can be decreased with increasing band degeneracy, this dependence is weak. For example, with $g_v = 6$, the contact resistivity is reduced by a factor of 1.82. Moreover, Eq. (6) also demonstrates that band anisotropy can lower ρ_c^{LL} by decreasing m_z (E_F further from the band edge) and increasing $m_{x,y}$ (larger number of conducting channels). Due to the effective mass power of 1/3, anisotropic effects are also weak. Finally, we verify the role of higher

energy bands. As an example, we consider a single lower energy (low m^*) band with six degenerate higher energy (large m^*) bands. In this case, only a factor of 2 reduction in ρ_c^{LL} is observed (see supplemental material for more details).[14] Hence, valley degeneracy, band anisotropy, and higher energy bands have only a modest impact on ρ_c^{LL}, leading to a reduction of 2–3 × under optimal conditions. This explains why such effects do not induce significant differences in the numerically calculated ρ_c^{LL}.

The markers in Figs. 3(a) and 3(b) show recent experimental values. InAs is known to produce very low ρ_c values, due to Fermi level pinning in the CB,[2] but our theoretical calculations indicate that it is possible to decrease ρ_c by another order of magnitude before reaching its intrinsic lower limit. Thus, there is room for improvement, which will be achieved by optimizing the physical properties at the metal/semiconductor interface to increase the transmission probability. The ITRS calls for $\rho_c = 10^{-9}$ Ω-cm^2 for 2023 and is plotted as the dashed horizontal line in Figs. 3(a) and 3(b). Our simulations demonstrate that the ITRS value is indeed possible, but sets a minimal carrier concentration in the range of approximately $2 \times 10^{19} - 5 \times 10^{19}$cm^{-3} depending on the semiconductor. Although this may not appear very restrictive, we note that this value represents the ideal case of perfect electronic transmission across the interface. In reality, higher carrier concentrations will be required to minimize the thickness of tunneling barriers and this may be a limitation for certain semiconductors, such as n-type GaSb with concentrations reaching $\sim 2 \times 10^{19}$cm^{-3}.

In this work, we have assumed a transmission $T(\epsilon)$ of one, however experimentally $T(\epsilon) < 1$ due to tunneling through a Schottky barrier and other non-idealities. When $T(\epsilon) \neq 1$, ρ_c^{LL} is calculated by introducing a factor $T(\epsilon)$ into the integral of Eq. (1). Using measured contact resistivity values, ρ_c^{exp}, the energy-averaged transmission is easily extracted using $\langle T \rangle = \rho_c^{LL}/\rho_c^{exp}$, where ρ_c^{LL} is simply calculated using Eq. (3). From the data shown in Figs. 3(a) and 3(b), we find $\langle T \rangle$ values in the range 1%–4% for $In_{0.53}Ga_{0.47}As$ and 10% for InAs. In practice, the properties of the interface determine the specific contact resistivity not the properties of the semiconductors alone.

In summary, the intrinsic lower limit for contact resistivity ρ_c^{LL} was calculated for InAs, $In_{0.53}Ga_{0.47}As$, GaSb, and Si using a full band ballistic quantum transport approach. Surprisingly, all calculated ρ_c^{LL} for fixed carrier density are found to be within a factor of 2–3 of each other, with Si and GaSb providing the smallest values. An analytical model, which is found to provide a very good fit to the numerical results, demonstrates that any reduction in ρ_c^{LL} achieved by increasing $M(\epsilon)$ is compensated by the fact that E_F will reside closer to the band edge. We also find that the value of $\rho_c = 10^{-9}$ Ω-cm^2 called by the ITRS for 2023 is in principle possible, but sets a minimal carrier concentration ranging from 2×10^{19}cm^{-3} to 5×10^{19}cm^{-3}. In reality, concentrations above this ideal value will be required. Experimentally, it is the specific interfacial properties of the metal/semiconductor junction, which determines how close ρ_c gets to its intrinsic lower limit. The contribution of this paper is to show how much improvement is possible through optimization of the metal/semiconductor interface.

J.M., C.J., and M.L. acknowledge support from the MSD focus center of the SRC and the Network for Computational Nanotechnology. Work at UCSB supported by the ONR under contract N00014-09-1-0231. J.M. thanks Professor Hong Guo for additional computational resources.

[1]M. J. W. Rodwell, M. Le, and B. Brar, Proc. IEEE **96**, 271 (2008).
[2]A. Baraskar, V. Jain, M. A. Wistey, U. Singisetti, Y. J. Lee, B. Thibeault, A. Gossard, and M. J. W. Rodwell, in 22nd International Conference on Indium Phosphide and Related Materials (IPRM), Takamatsu, Japan, 31 May-4 June (2010), pp. 1–4.
[3]International Technology Roadmap for Semiconductors 2011 Edition, Front End Processes, http://www.itrs.net/.
[4]A. Baraskar, A. C. Gossard, and M. J. W. Rodwell, in 24th International Conference on Indium Phosphide and Related Materials (IPRM), Santa Barbara, USA, 27–30 August (2012).
[5]S. Datta, *Electronic Transport in Mesoscopic Systems* (Cambridge University Press, New York, 1995).
[6]C. Jeong, R. Kim, M. Luisier, S. Datta, and M. Lundstrom, J. Appl. Phys. **107**, 023707 (2010).
[7]E. O. Kane, J. Phys. Chem. Solids **1**, 249 (1957).
[8]S. Steiger, M. Povolotskyi, H.-H. Park, T. Kubis, and G. Klimeck, IEEE Trans. Nano **10**, 1464 (2011).
[9]G. Kresse and J. Furthmüller, Phys. Rev. B **54**, 11169 (1996); P. E. Blochl, *ibid.* **50**, 17953 (1994).
[10]J. P. Perdew, K. Burke, and M. Ernzerhof, Phys. Rev. Lett. **77**, 3865 (1996).
[11]N-InGaAs: A. Baraskar, M. A. Wistey, V. Jain, U. Singisetti, G. Burek, B. J. Thibeault, Y. J. Lee, A. Gossard, and M. J. W. Rodwell, in 51st Electronic Materials Conference (EMC), State College, USA, 24-26 June (2009); J. Vac. Sci. Technol. B **27**, 2036 (2009). P-InGaAs: E. Lobisser, A. Baraskar, V. Jain, B. Thibeault, A. Gossard, and M. J. W. Rodwell, in 38th International Symposium on Compound Semiconductors, Berlin, Germany, 22–26 May (2011); in 28th North American Molecular Beam Epitaxy Conference, San Diego, USA, 14–17 August (2010); A. Baraskar, V. Jain, M. A. Wistey, B. Thibeault, A. Gossard, and M. J. W. Rodwell, in 16th International Conference on Molecular Beam Epitaxy, Berlin, Germany, 22–27 August (2010); A. Baraskar, V. Jain, M. Wistey, E. Lobisser, B. Thibeault, Y. J. Lee, A. Gossard, and M. J. W. Rodwell, in 52nd Electronics Materials Conference (EMC), Notre Dame, USA, 23–25 June (2010).
[12]N-GaSb: K. Ikossi, M. Goldenberg, and J. Mittereder, Solid-State Electron. **46**, 1627 (2002). P-GaSb: J. I. Chyi, J. Chen, N. S. Kumar, C. Kiely, C. K. Peng, A. Rockett, and H. Morkoc, Appl. Phys. Lett. **55**, 570 (1989).
[13]N. Stavitski, M. J. H. van Dal, A. Lauwers, C. Vrancken, A. Y. Kovalgin, and R. A. M. Wolters, IEEE Electron Device Lett. **29**, 378 (2008).
[14]See supplementary material at http://dx.doi.org/10.1063/1.4798238 for an assessment of the parabolic and non-parabolic approximations, the zero temperature approximation and the effect of higher energy bands using the analytical contact resistivity.